Title

Three Dimensional Deformation Comparison of Self-ligating Brackets

Authors

Garrett W. Melenka, BSc[a].; David S. Nobes,PhD[b]; Jason P. Carey, PhD[c]; Paul W. Major, DDS, MSc, FRCD(C)[d];

[a]Garrett W. Melenka, BSc, Graduate Student, Mechanical Engineering, Faculty of Engineering, University of Alberta, Edmonton, Alberta, Canada

[b]David S. Nobes, Assistant Professor, Mechanical Engineering, Faculty of Engineering, University of Alberta, Edmonton, Alberta, Canada

[c]Jason P. Carey, Professor, Mechanical Engineering, Faculty of Engineering, University of Alberta, Edmonton, Alberta, Canada

[d] Professor and Chair, Department of Dentistry, Faculty of Medicine and Dentistry

Corresponding Author

Dr. Paul W. Major

Professor and Chair, Department of Dentistry, Faculty of Medicine and Dentistry

5478 Edm Clinic Health Academy

Faculty of Medicine and Dentistry

University of Alberta

Edmonton, AB

Telephone: (780) 492-3312

Fax: (780) 492-1624

Email: major@ualberta.ca

Abstract

Introduction: Archwire rotation is used in orthodontic treatment to alter the labial-lingual orientation of a tooth. Measurement of the three dimensional (3D) motion of the orthodontic brackets requires a new configuration of the Orthodontic Torque Simulator (OTS).

Methods: The OTS was coupled with a stereo microscope and two cameras in order to allow for the three dimensional bracket motion to be detected during wire twisting. The stereo camera images was processed using a 3D DIC technique in order to determine the 3D deformation or the orthodontic brackets. Three self-ligating brackets (Damon Q, In-Ovation R and Speed) were compared using the 3D DIC method to demonstrate the difference in 3D motion of self-ligating brackets components.

Results: Contour plots of the three brackets demonstrate the 3D motion of the bracket tie-wings as well as the archwire retentive component. The 3D motion of the bracket tie-wings was quantified.

Conclusions: The 3D DIC method utilized to quantify bracket deformation has shown the 3D motion of the bracket tie-wings as well as the motion of the archwire retentive component. This measurement technique can be used to evaluate brackets of varying design.

Keywords: Digital Image Correlation, orthodontic bracket, deformation

1. **Introduction**

Archwire rotation is used in edgewise orthodontic treatment to alter the labial-lingual orientation of a tooth through the interaction of a rectangular archwire and bracket slot [1]. Tooth movement is achieved through pressure applied to the tooth by the archwire [1, 2]. The resulting tooth movement depends highly on the magnitude of torsion applied through archwire rotation; the material properties of the archwire and bracket; bracket and archwire geometry; and the location of the bracket on the tooth [3-5]. The aforementioned factors will greatly affect the speed and efficacy of treatment since a large torque applied to the archwire can result in permanent deformation to the bracket tie wings [3]. The occurrence of permanent deformation to the orthodontic brackets will cause the bracket to cease to function as expected and consequently treatment time could be affected [6]. Therefore, it is desirable to quantify the motion of bracket tie-wings due to archwire rotation.

An Orthodontic Torque Simulator (OTS) has been designed to simulate the clinical situation of archwire rotation as presented by Badawi et al. [7]. The OTS was expanded upon though the development of an optical method of measuring bracket deformation by Lacoursiere et al. [6]. The optical bracket deformation method has indicated that the loads applied to an orthodontic bracket through archwire rotation can result in both plastic and elastic deformation. The optical bracket deformation method utilizes digital image correlation (DIC) to determine the motion of the bracket tie-wings. DIC is a well established optical measurement technique that has been widely used for both displacement and strain measurement [8-14]. DIC has been applied to the field of orthodontics to measure the shrinkage of resin based dental composites [15]. The optical bracket deformation measurement method developed by Lacoursiere et al.[6] has since been used to measure the deformation of both conventional brackets and self-ligating bracket [16-18].

The measurement of bracket tie-wing deformation using a single camera is limited to only measuring two-dimensional (2D) of the brackets. The study by Major et al. [16] compared the 2D deformation of three self-ligating brackets and determined that In-Ovation R plastically deform less than Speed and Damon Q brackets for a maximum torquing angle of 63°. Orthodontic brackets and archwires move and interact in three dimensions (3D) therefore it is necessary to determine if significant motion of the orthodontic brackets occurs in all three-dimensions. The addition of a second camera will allow for the 3D motion of the orthodontic brackets to be measured using a 3D DIC technique [14, 19-21] to demonstrate if significant motion in all 3 directions exists. The ability to measure 3D deformation of orthodontic bracket will enable for the archwire-bracket interaction to be fully described.

The addition of a second camera to the OTS measurement system will also allow for the motion of the movable component used to secure the archwire of self-ligating brackets to be measured [22, 23]. The movable component used to secure the archwire is often referred to as a spring clip or slide depending on the bracket design [24, 25] but for the remainder of this discussion the movable component will be referred to as the archwire retentive component (ARC). Measurement of the ARC motion will allow for comparison of active and passive ligation brackets designs. Currently the motion of the ARC has not been evaluated to determine if compliance of active and passive ligation ARC designs can affect treatment [25-27]. The goal of this study is to examine the deformation of self-ligating brackets in three dimensions using the 3D DIC version of the OTS and the motion of the ARC.

2. **Methods and Materials**

A schematic of a tooth, self-ligating bracket and archwire is shown in Figure 1. Figure 1 (a) and (b) shows the coordinate system assigned to the bracket (x^*,y^*,z^*) where the x^* axis is defined as parallel to the archwire, the y^* axis is defined as the direction of lateral motion of the bracket tie wings due to archwire rotation and the z^* axis defines the direction from the base of the orthodontic bracket to the top of the bracket tie wings. This coordinate system will be used to quantify the deformation that occurs to the bracket due to archwire rotation. Archwire rotation occurs about the x^* axis and the angle of archwire rotation is defined as ϕ. The angle of archwire rotation, ϕ, is shown in Figure 1 (c). The neutral position of the archwire is defined as when the archwire is parallel to the base of the bracket slot in Figure 1 (c).

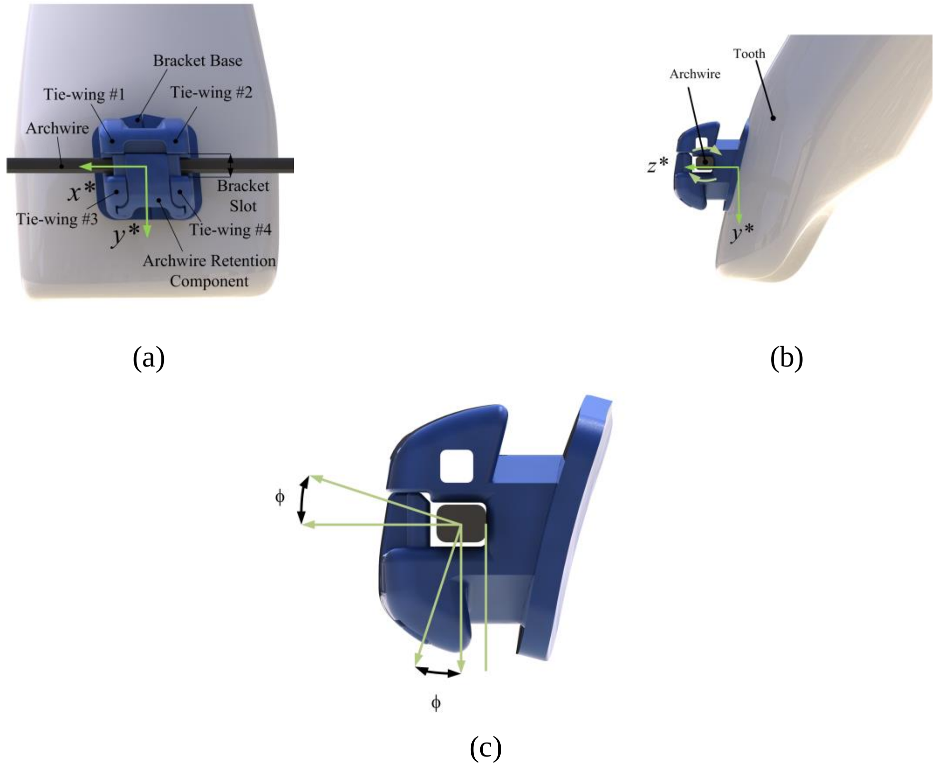

Figure 1: Self-ligating orthodontic bracket components (a) Top view of bracket showing tie-wings, archwire and bracket base (b) Side view of bracket showing the angle of the bracket slot (prescription). Archwire rotation occurs about the x^* axis of the bracket coordinate system. (c) Control of tooth angulations using archwire rotation (d) Archwire rotation, ϕ.

Archwires are maintained in the bracket slot using two main methods: elastomeric or steel ligatures or self-ligating brackets. Self-ligating brackets are advantageous as the archwire can be ligated in the bracket slot more quickly than conventional elastic or steel ligation [25, 26]. As well, the ARC is not prone to degradation like elastic ligatures due to the temperature and chemistry within the mouth [26]. Active and passive self-ligating brackets will be compared using the 3D OTS to show the 3D motion of the bracket tie-wings and the motion of the ARC.

Top and side images of three orthodontic brackets are shown in Figure 2 to demonstrate the difference between active and passive ligation bracket designs. These images show the irregular geometries of these particular self-ligating brackets. The brackets shown are Damon Q (Ormco Corporation, Orange, California, USA), Speed (Strite Industries, Cambridge, Ontario, Canada), and In-Ovation R (GAC, Bohemia, NY, USA) self-ligating brackets. The In-Ovation R and Speed brackets are active ligation brackets while the Damon Q is a passive ligation bracket. Active ligation brackets are designed with a curved leaf spring type ARC which applies force to the archwire [28]. The ARC for active ligation brackets encroaches in the bracket slot to maintain contact with the archwire [28]. Contact between the archwire and ARC will help to maintain the alignment of the wire in the brackets slot. A disadvantage of the active ligation brackets is the possibility of reduced torque transmitted to the tooth due to reduced gingival slot wall depth to allow for the elastic ARC to secure the archwire in the bracket slot [25]. The curved leaf spring ARC is shown in the side images of the In-Ovation R and Speed brackets. Passive ligation brackets have a more rigid ARC that does not maintain contact with the archwire [28].

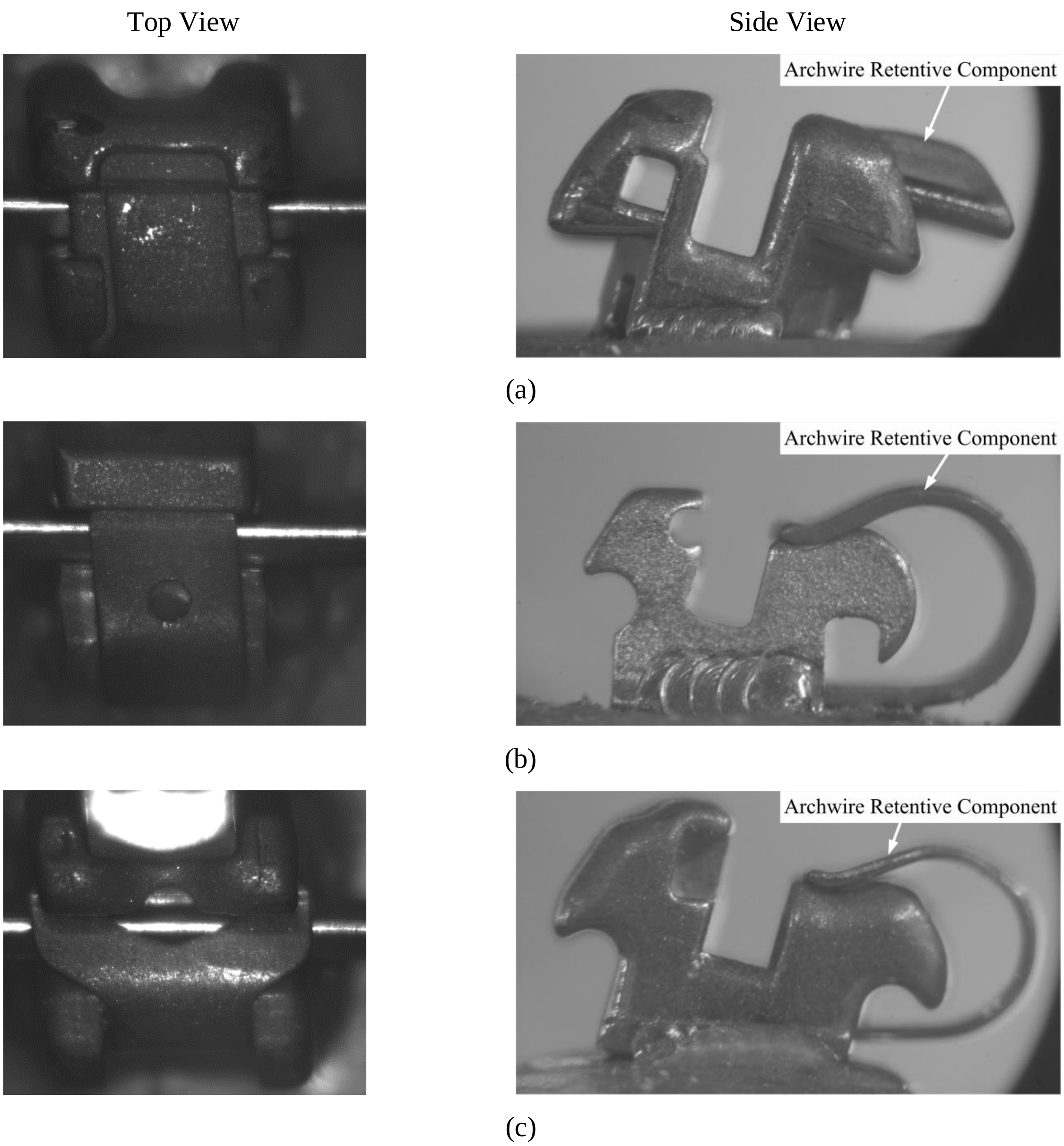

Figure 2: Top and Size views of orthodontic brackets (a) Damon Q (b) Speed (c) Innovation R

A comparison of active and passive ligation brackets is shown in Figure 3. Figure 3 (a) shows that there is clearance between the archwire and the ARC for the Damon Q bracket while in Figure 3 (b) the ARC is in contact with the archwire.

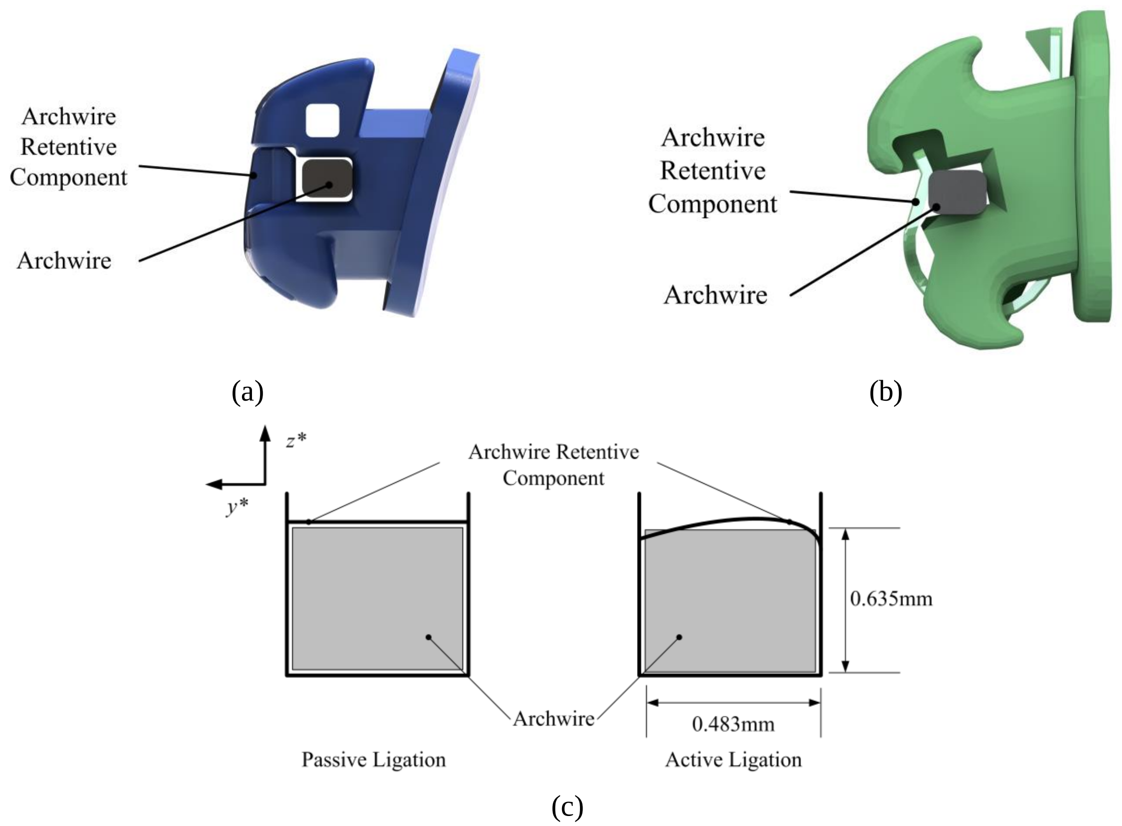

Figure 3: Comparison of self-ligating brackets (a) passive ligation Damon Q (solid model provided by Ormco) (b) In-Ovation R (solid model provided by GAC) active ligation applies a preload to the wire. (c) schematic of passive and active ligation brackets

The 3D deformation of orthodontic brackets was measured using a modified version of the OTS [6, 7]. The 3D DIC measurement version of the OTS is shown in Figure 4. A computer controlled stepper motion (Cool Muscle CM1-C-11L30, Myostat Motion Control Inc., Newmarket, ON, Canada) and gear box rotates the archwire in the bracket. Two dies, that clamp the archwire, are mechanically locked together by a yoke provide support to the archwire and even rotation from both sides. Also shown in this figure is the 6-axis load cell (Nano17 SI-25-0.25, ATI Industrial Automation, Apex, NC, USA) used to collect force and moment data applied to an orthodontic bracket due to archwire rotation. Control of the OTS stepper motor, acquisition of data from the load cell and image acquisition is automated using custom designed software (LabWindows/ CVI, National Instruments, Austin TX). The complete details of the OTS design and description of the archwire rotation mechanism is described by [6, 7, 16-18].

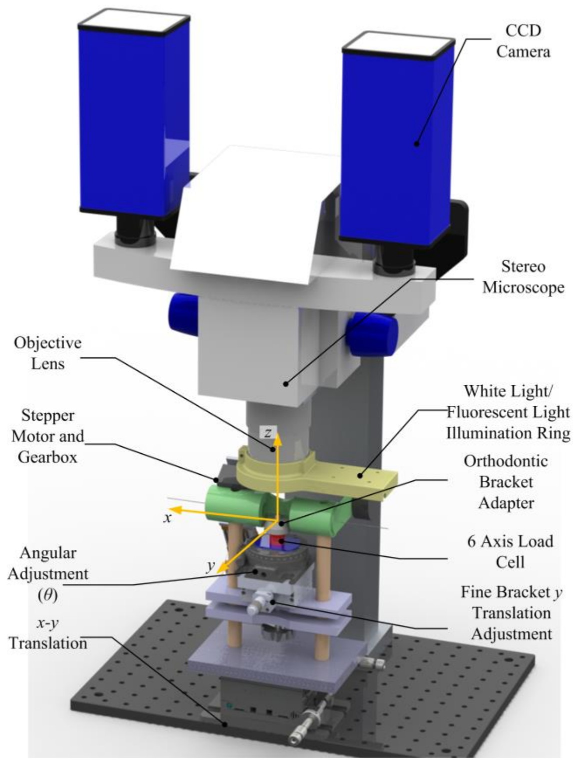

Figure 4: Orthodontic Torque Simulator

The image acquisition system shown in Figure 4 collects images of orthodontic brackets using a stereo microscope (Zeiss SteREO Discovery v8 microscope Carl Zeiss Micro Imaging GmbH Göttingen, Germany) with a 60mm working distance objective lens (1.0X Zeiss V8 Plan Apo Objective Lens**,** Zeiss MicroImaging GmbH Göttingen, Germany). Images were collected using two CCD cameras (Imager Intense, LaVision GmbH, Göttingen, Germany) at 1376×1040 pixels and 12-bit resolution. The cameras were connected to the stereo microscope using an intermediate phototube (Intermediate Phototube S 50:50 ports, Zeiss MicroImaging GmbH Göttingen, Germany). The brackets were imaged at 2.0x magnification to maximize the bracket in the camera field of view. Test specimens were illuminated using a ring light (2.64" Ring Light, Variable Frequency, Edmund Optics, Barrington, NJ, USA) and a 365nm black-light (Black (365nm Peak) Replacement Bulb, Edmund Optics, Barrington, NJ, USA) to provide even illumination across the field of view.

A stainless steel bracket cylinder with a 9.0mm nominal diameter was used as an analog for a tooth as described by Badawi et al. [7] and the brackets were mounted to the cylinder using an epoxy (Loctite E-20HP; Hysol, Henkel, Rocky Hill, Conn.). Cylinders were used to transmit the loads applied to the orthodontic bracket by the archwire to a 6-axis load cell and to allow for free rotation of the archwire in the bracket slot.

Images collected using the OTS were acquired and post processed using a commercial software package (StrainMaster 3D, LaVision GmbH DaVis 8.06. Gottingen, Germany, 2009). Image subsets, or window size, used to determine the 3D displacement of the brackets were 64x64 pixels as a compromise between vector precision and maximization of the number of interrogation windows for each tie-wing [29]. The field of view for the brackets was 1376 x 1040 pixels or 4.25 x 3.2 mm therefore the resolution for this camera setup with a 64x64 subset size will be 0.07μm [29]. DIC displacement measurement comprises of four consecutive steps (1) specimen preparation (2) calibration of the imaging system for a defined field-of-view (3) collection of specimen deformation before and after loading, and (4) post processing of images to determine displacement or strain [30]. A specimen is prepared by applying a random pattern to the object surface. Images are calibrated to convert from pixels to physical space (e.g. mm, inches) by acquiring an image of a target with a grid of known spacing. Each digital image is segmented into evenly spaced subsets and an image correlation algorithm is performed for each image subset. Deformation is measured by tracking contrast features on the specimen surface between subsequent images. The displacement of a subset is determined by maximizing a cross-correlation equation for the images collected before and after deformation [10, 30].

Orthodontic brackets were prepared prior to testing by coating the surface of the bracket with fluorescent airbrush paint (5404 Fluorescent Green Createx Airbrush Colors, Createx Colors, East Granby CT). The speckle pattern was applied using an airbrush (Custom Micron B, Iwata Medea Inc. Portland OR). The paint was reduced at a ratio of approximately 2:1 to improve the flow of the paint through an airbrush (Wicked W100 Reducer Createx Airbrush Colors, Createx Colors, East Granby CT). Fluorescent paint was chosen for the speckle pattern to reduce reflection from the metallic bracket surfaces which can introduce errors in the DIC image processing. The use of an airbrush and fluorescent particles for DIC was described by Berfield et al. [31]. Previously, bracket deformation measurements have used a micro-etcher to produce a random speckle pattern on the bracket surface [7-9] but the fluorescent paint allows for a speckle pattern to be produced on the surface of the brackets without affecting the material properties of the bracket.

Deformation of the bracket will be assessed by determining the relative motion between the four bracket tie-wings shown in Figure 5. Figure 5 shows the bracket tie-wing and ARC regions for the Damon Q, In-Ovation R and Speed brackets. The displacement vector fields generated using the 3D DIC software were further processed using a custom code to determine the motion of the bracket tie-wings and ARC (MATLAB, 2009a, The MathWorks Inc., Natick, MA, U.S.A.). Figure 5 also shows the 64x64 pixel subset which was used for the measurement of the 3D displacement of the bracket. Equation (1) details the calculation of the bracket displacement in the x^*, y^* and z^* directions. In this equation $\overline{D_{TieWing}}$

denotes the average displacement of the defined regions for tie-Wings 1,2,3, and 4 for the i=x*,y*,z* directions. LHS_D is the displacement between tie-wings 1 and 3 while RHS_D is the displacement between tie-wings 2 and 4.

$$
\begin{aligned}
LHS_{D_i} &= \left[\overline{D_{TieWing1}} - \overline{D_{TieWing3}}\right]_i \\
RHS_{D_i} &= \left[\overline{D_{TieWing2}} - \overline{D_{TieWing4}}\right]_i
\end{aligned}
\tag{1}
$$

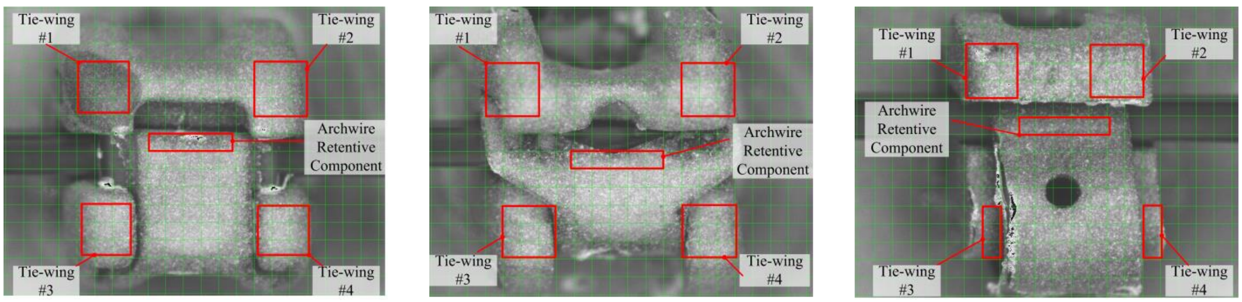

(a) (b) (c)

Figure 5: Orthodontic bracket box regions used to track tie-wing motion (a) Damon Q (b) In-Ovation R (c) Speed

In addition, the motion of the bracket ARC in the i=x*,y*,z* directions was measured. Bulk motion of the entire bracket was eliminated to find the relative motion of the ARC by subtracting the average displacement of the tie wings from the motion of the bracket retentive component. The relative ARC motion is denoted as $RelativeARC_i$ and the retentive component motion is denoted as ARC_i as shown in Equation (2).

$$
RelativeARC_i = ARC_i - \left[\frac{1}{4}\sum_{j=1}^{4}\overline{D_{TieWing\,j}}\right]_i
\tag{2}
$$

Three self-ligating orthodontic brackets were used in this study. A total of 30 brackets were tested, ten Damon Q (Ormco Corporation, Orange, California, USA) and 10 In-Ovation R (GAC, Bohemia, NY, USA) brackets and 10 Speed (Strite Industries, Cambridge, Ontario, Canada). All brackets are maxillary right incisor (U1R) with a nominal slot width of 0.5588mm(0.022”). All brackets were selected to have comparable medium torque prescriptions. The Damon Q brackets have a prescription of 15º torque, 5 º angle and 0 º rotation while the Speed and In-Ovation brackets have a prescription of 17º torque, 5 º angle and 0 º rotation. The archwire (Ormco, Orange, California, USA) used for this investigation had a 0.483 x 0.635mm (0.019 x 0.025”) cross section.

Using the automated OTS software the angle of the archwire, ϕ, was rotated in 3° increments to a maximum angle of 45°. Once the maximum angle was reached the archwire was returned to the original position in 3° increments. At each increment a pair of stereo images of the orthodontic bracket was collected resulting in thirty-two (32) image pairs collected. The stereo image sequence was used to measure the 3D deformation of the bracket due to archwire rotation by post processing the images using the previously described 3D DIC method. Deformation of the orthodontic bracket and the 3D displacement vectors were visualized using a scientific visualization software package (ParaView, Kitware, Inc. Clifton Park, New York). The visualization software package was used to view the result of the bracket-archwire interaction in three dimensions.

Example images collected of a Damon Q bracket are shown in Figure 6. The sequence shows increasing archwire rotations (ϕ) of 0, 21, and 45° as well as decreasing archwire rotation of 21 and 0°. The image sequence shows a number of features that materialize for archwire rotation in the bracket slot. These features include the changing aspect of the archwire due to rotation and the widening of the gap between the ARC and the top tie-wings (as shown in the image) which is a result of the widening of the bracket slot due to applied torque. Image sequences, like the one shown in Figure 6, will be post-processed using the LaVision 3D DIC software in order to determine the 3D motion of the bracket tie-wings and ARC.

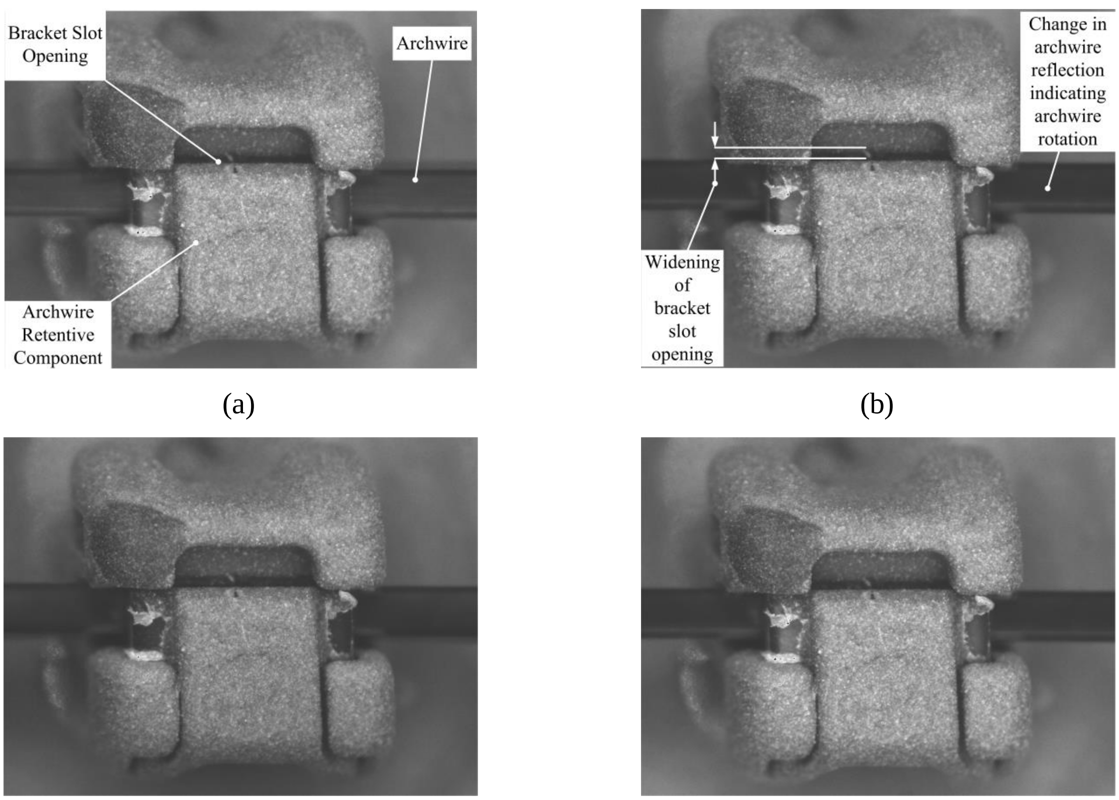

(a) (b)

(c) (d)

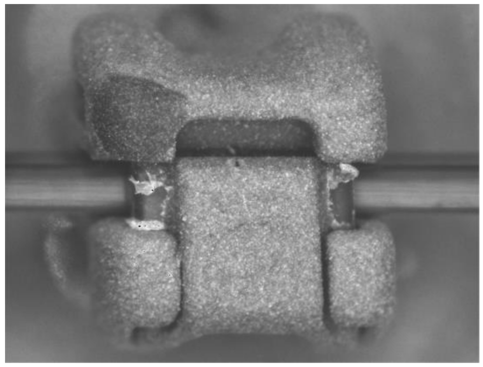

(e)

Figure 6: Damon Q orthodontic bracket deformation due to archwire rotation (ϕ) (a) increasing 0° (b) increasing 21° (c) increasing 45° (d) decreasing 21° (e) decreasing 0° 3D DIC bracket deformation.

Images of self-ligating brackets collected using the stereo-microscope version of the OTS are shown in Figure 7. Also shown are the 3D surfaces generated from the 3D DIC measurement method for comparison. The ParaView surfaces will be used to indicate visualize the motion of the brackets. Figure 7 shows that the 3D bracket geometry can be reconstructed from stereo images pairs collected using the 3D OTS.

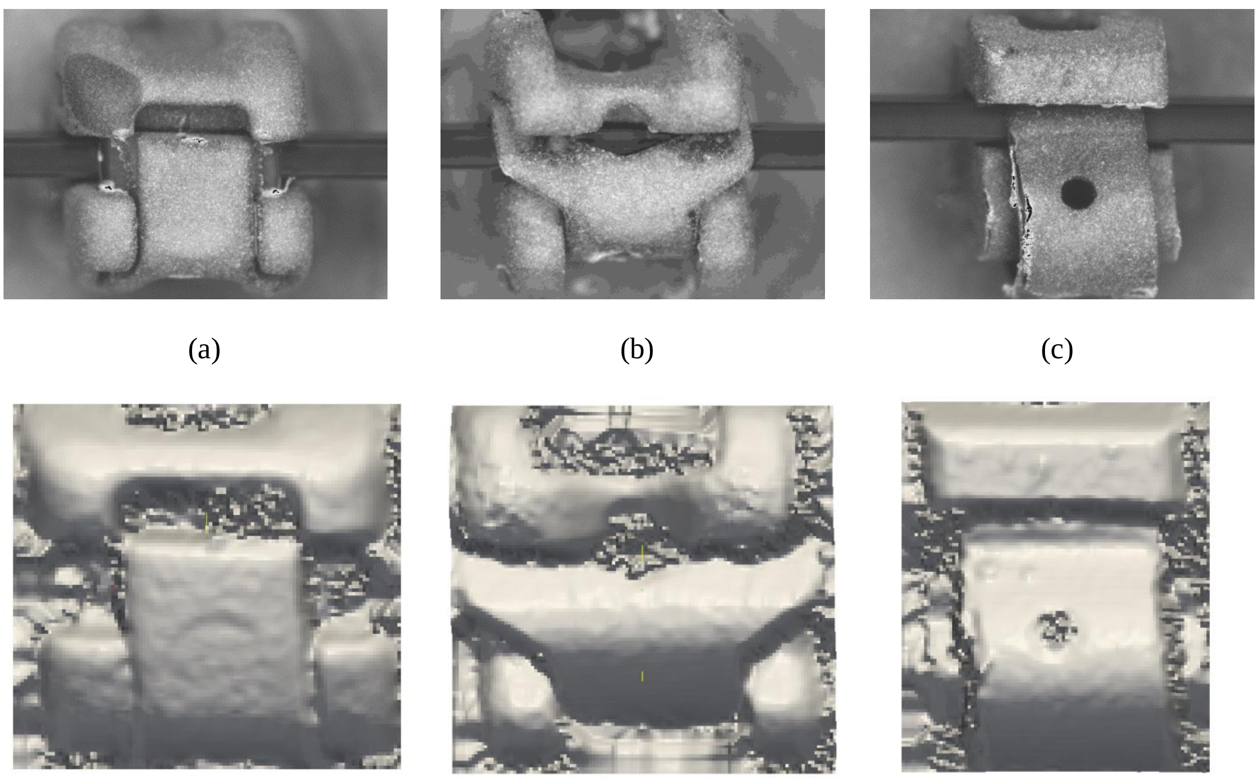

(a) (b) (c)

(d) (e) (f)

Figure 7: Orthodontic bracket ParaView surfaces (a) Damon Q (b) In-Ovation R (c) Speed (d) Damon Q ParaView Surface (e) In-Ovation R ParaView surface (f) Speed ParaView surface.

The original image and ParaView surface of an In-Ovation R bracket are compared in Figure 8. Three regions are highlighted (a,b,c) in this figure. The highlighted regions indicate where the bracket image is out-of-focus. The out-of-focus regions from the original bracket image result in uneven surfaces in the ParaView images shown in Figure 8 (b). Regions a and c correspond to the out-of-focus bracket base and region b corresponds to the archwire. The uneven surface in region b occurs since a speckle pattern was not applied to the archwire; therefore no DIC displacement or surface data can be obtained from this region. The regions a,b,c in Figure 8 will not be evaluated to determine bracket deformation.

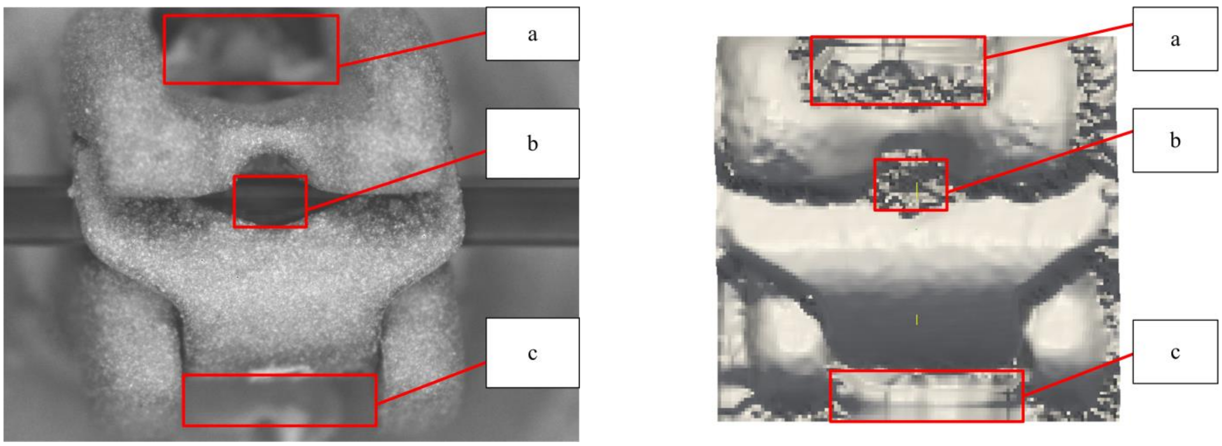

(a) (b)

Figure 8: In-Ovation R bracket image and ParaView surface comparison (a) original bracket image (b) ParaView surface

The bracket deformation results collected using the 3D OTS will be compared using a Mann-Whitney U nonparametric test (ranksum function, Statistics Toolbox, MATLAB, 2009a, The MathWorks, Natick, MA, U.S.A.) to determine if a statistically signification difference can be found between the brackets. The test was selected due to the small sample size for each bracket. A *P*-value of less than 0.05 is the criteria that will indicate if a statistical difference exists between the two brackets.

3. **Results**

Representative image sequences of the Damon Q, In-Ovation R and Speed brackets will be compared to visualize 3D bracket deformation due to archwire rotation. A sequence of images of a Damon Q bracket is shown in Figure 9 for selected angles as the archwire was progressively rotated from 0 to 45° in 3° increments. The change in wire angle can be seen in each successive image.

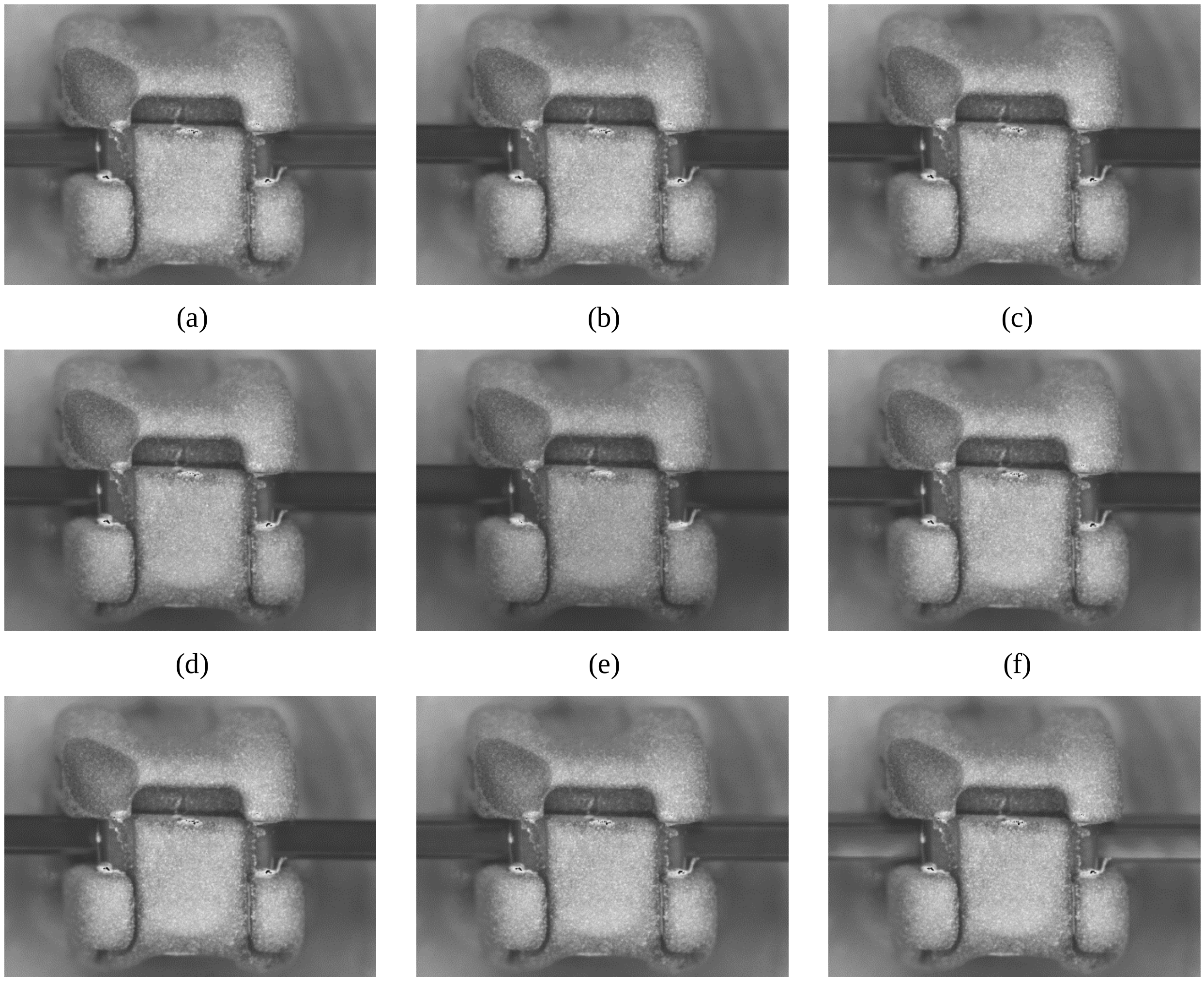

(a) (b) (c) (d) (e) (f) (g) (h) (i)

Figure 9: Damon Q image sequence (a) 0 degree (b) 9 degree (c) 21 degree (d) 33 degree (e) 45 degree (f) -33 degree (g) -21 degree (h) -9 degree (i) -0 degree

The same image sequence shown in Figure 9 was processed using the 3D DIC method and then visualized using ParaView. The image sequences in Figure 10, Figure 11 and Figure 12 show the displacement field in the x^*,y^* and z^* directions. In these sequences red indicates maximum deformation while green indicates zero deformation. These figures show that the maximum displacement of occurred at a wire rotation of 45°. The image sequence also shows the increase and decrease in tie-wing motion as the wire is rotated to a maximum angle of 45° and then returned to the origin. The original image sequences in Figure 9 and 3D surfaces in Figure 10, Figure 11 and Figure 12 show that images collected using the 3D OTS can be collected and processed to visualize bracket deformation due to archwire rotation.

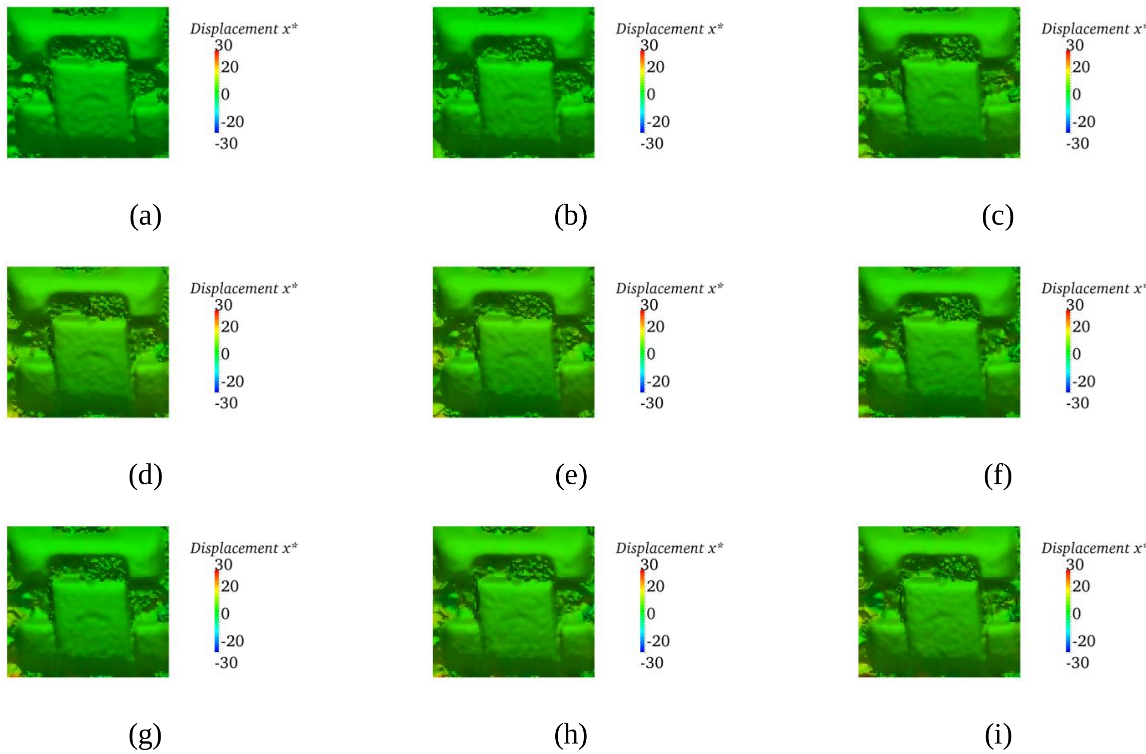

Figure 10: Damon Q ParaView image sequence *x displacement (a) 0 degree (b) 9 degree (c) 21 degree (d) 33 degree (e) 45 degree (f) -33 degree (g) -21 degree (h) -9 degree (i) -0 degree. Displacement measured in micrometers (µm)**

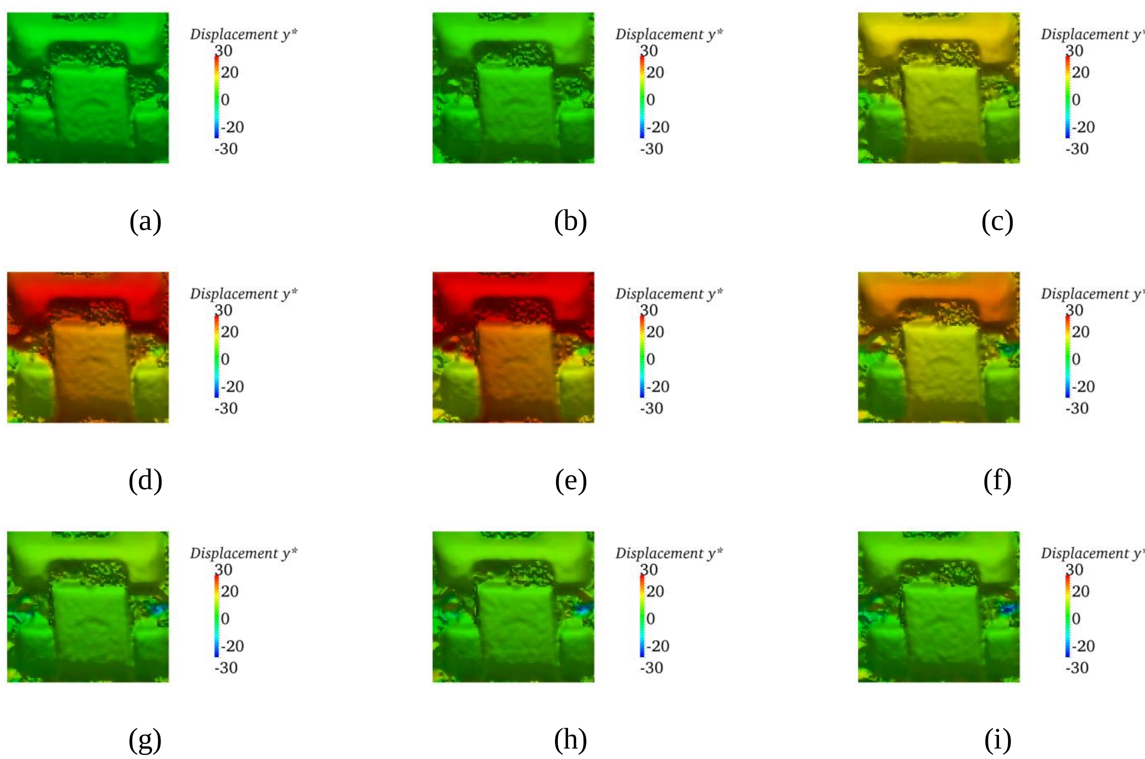

Figure 11: Damon Q ParaView image sequence *y displacement (a) 0 degree (b) 9 degree (c) 21 degree (d) 33 degree (e) 45 degree (f) -33 degree (g) -21 degree (h) -9 degree (i) -0 degree. Displacement measured in micrometers (µm)**

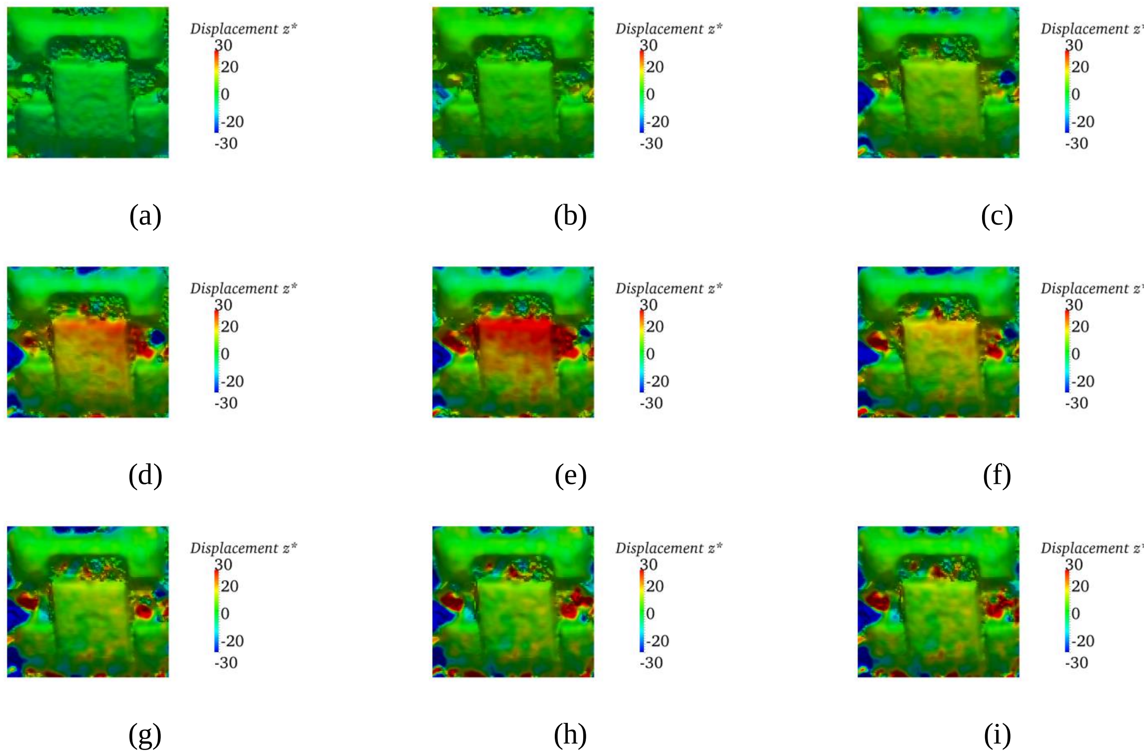

Figure 12: Damon Q ParaView image sequence x^* displacement (a) 0 degree (b) 9 degree (c) 21 degree (d) 33 degree (e) 45 degree (f) -33 degree (g) -21 degree (h) -9 degree (i) -0 degree. Displacement measured in micrometers (µm)

Similarly, an image sequence of a typical In-Ovation R bracket is show in Figure 13. The corresponding 3D surface and deformation of the In-Ovation R bracket is shown in Figure 14, Figure 15, and Figure 16. The image sequences again indicate that the maximum displacement occurred for a wire rotation of 45°.

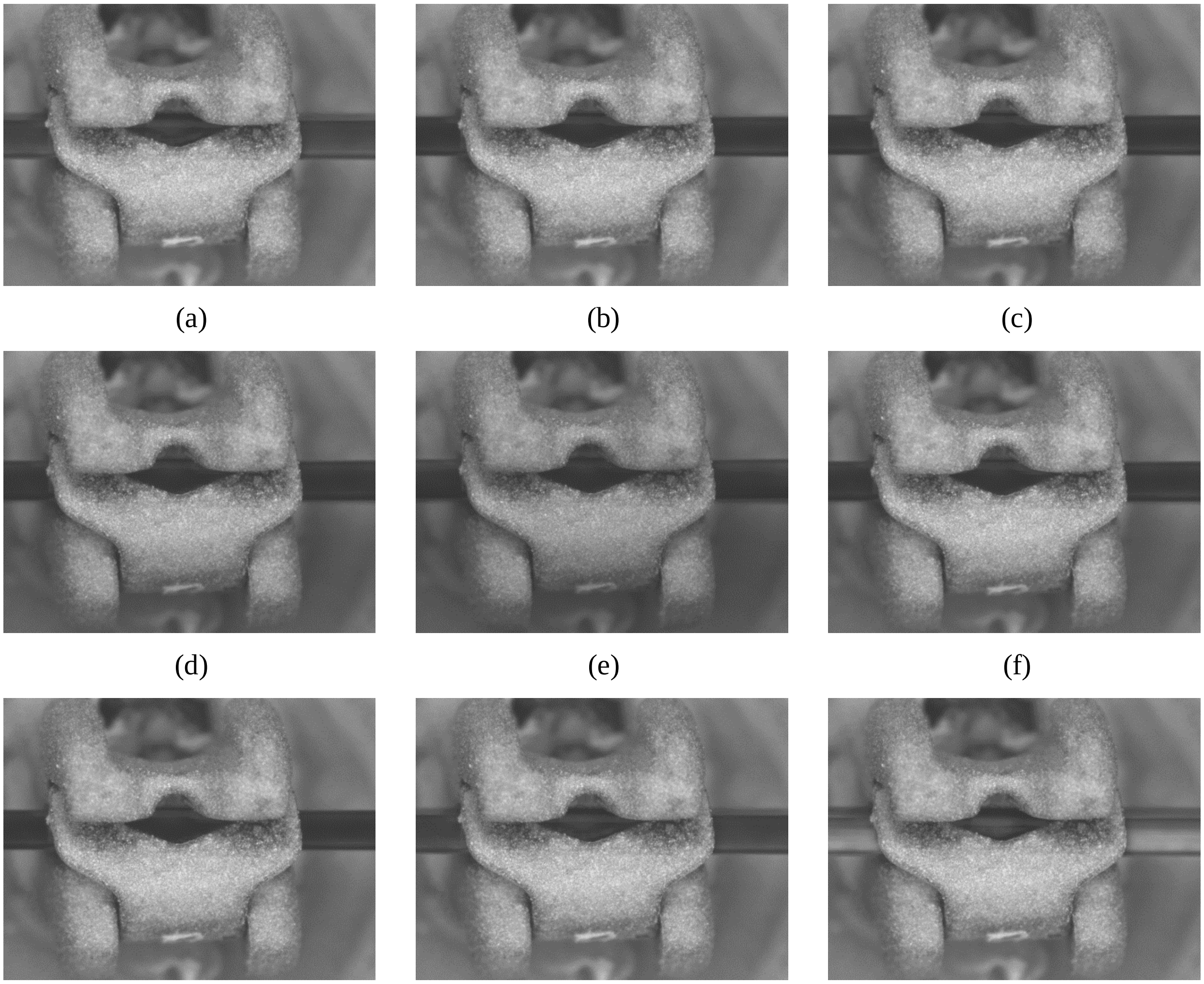

(a) (b) (c)

(d) (e) (f)

(g) (h) (i)

Figure 13: In-Ovation R image sequence *y displacement (a) 0 degree (b) 9 degree (c) 21 degree (d) 33 degree (e) 45 degree (f) -33 degree (g) -21 degree (h) -9 degree (j) -0 degree**

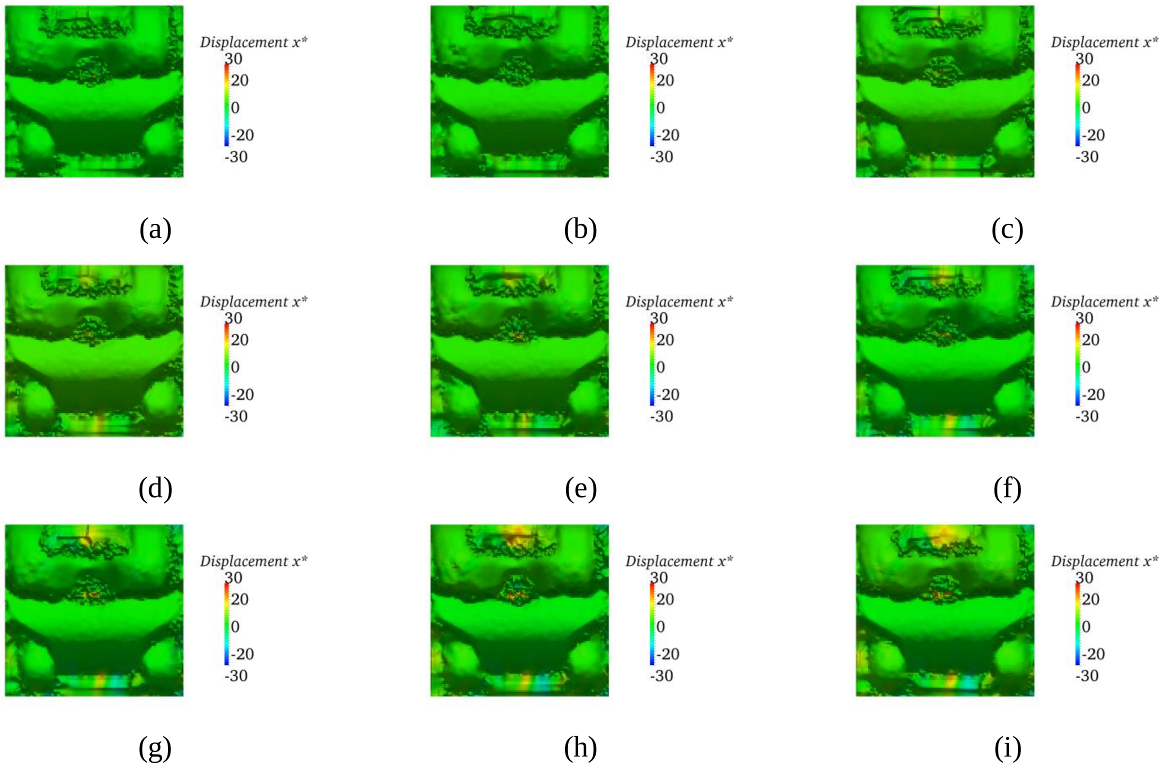

Figure 14: In-Ovation R ParaView image sequence *x displacement (a) 0 degree (b) 9 degree (c) 21 degree (d) 33 degree (e) 45 degree (f) -33 degree (g) -21 degree (h) -9 degree (i) -0 degree. Displacement measured in micrometers (µm)**

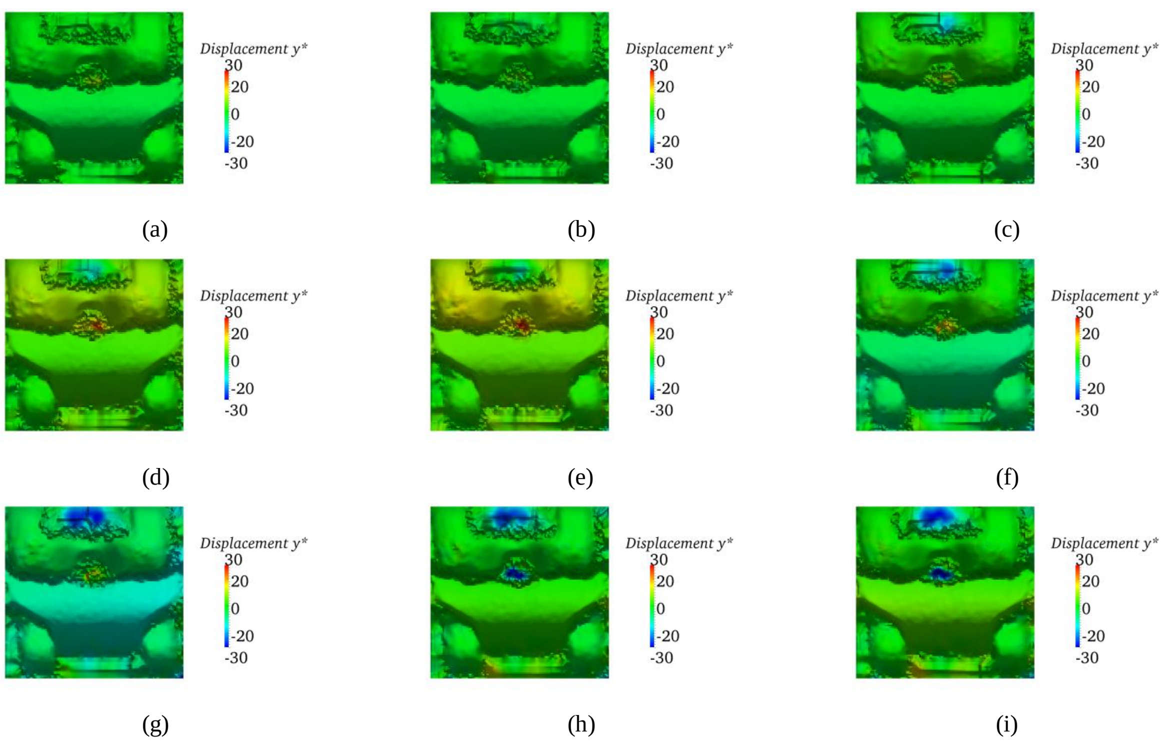

Figure 15: In-Ovation R ParaView image sequence *y displacement (a) 0 degree (b) 9 degree (c) 21 degree (d) 33 degree (e) 45 degree (f) -33 degree (g) -21 degree (h) -9 degree (j) -0 degree. Displacement measured in micrometers (µm)**

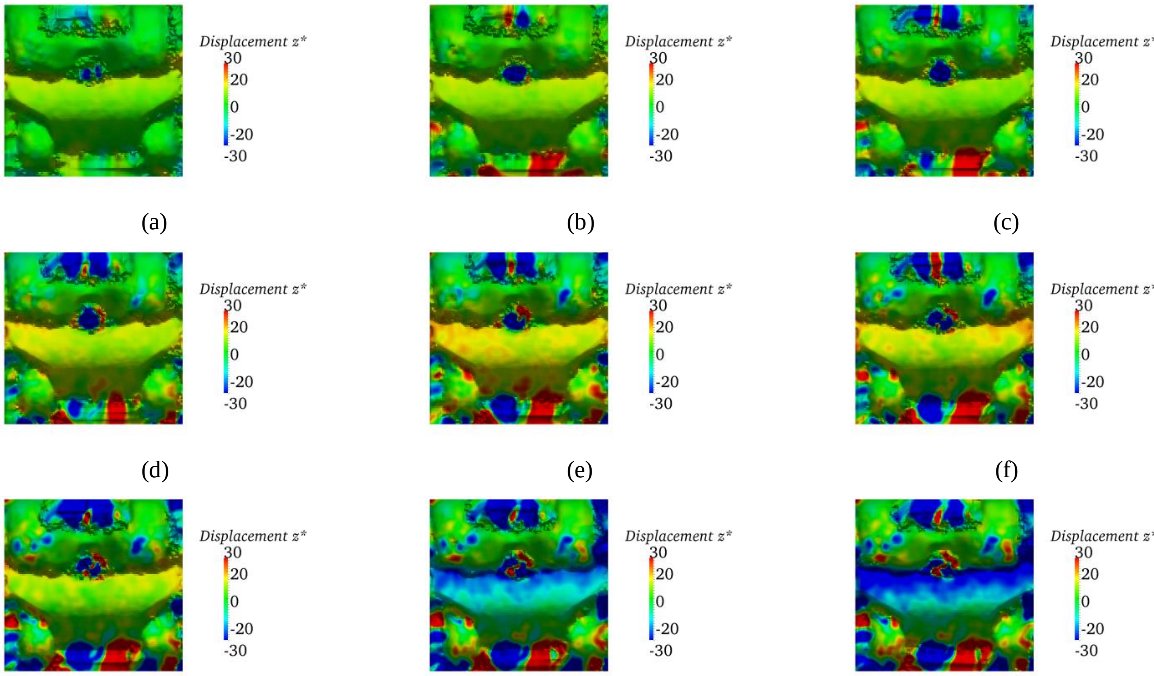

(a) (b) (c)

(d) (e) (f)

(g) (h) (i)

Figure 16: In-Ovation R ParaView image sequence *z displacement (a) 0 degree (b) 9 degree (c) 21 degree (d) 33 degree (e) 45 degree (f) -33 degree (g) -21 degree (h) -9 degree (j) -0 degree**

An image sequence of a Speed bracket was also processed and visualized for comparison with the Damon Q and In-Ovation R brackets. The original image sequence of the Speed bracket is shown in Figure 17 and the resultant 3D surface and displacement is shown in Figure 18, Figure 19 and Figure 20. The image sequence of the Speed bracket in Figure 17 shows a bracket where the ARC opened during testing. The opening of the ARC during testing is also shown in the resulting contour plots in Figure 18, Figure 19 and Figure 20.

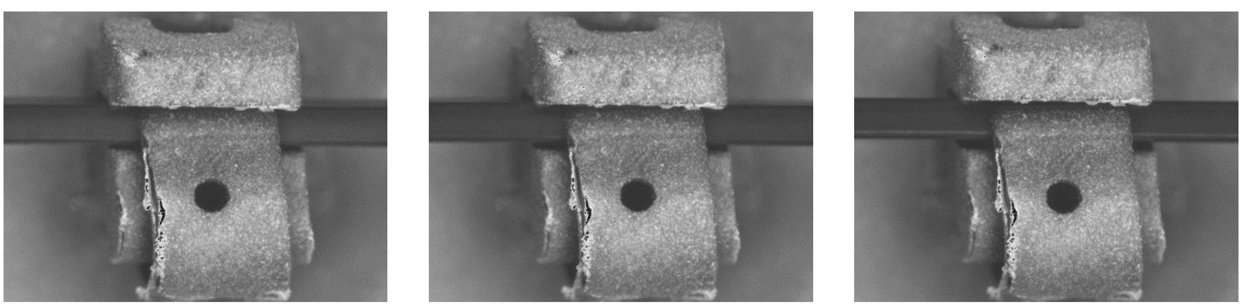

(a) (b) (c)

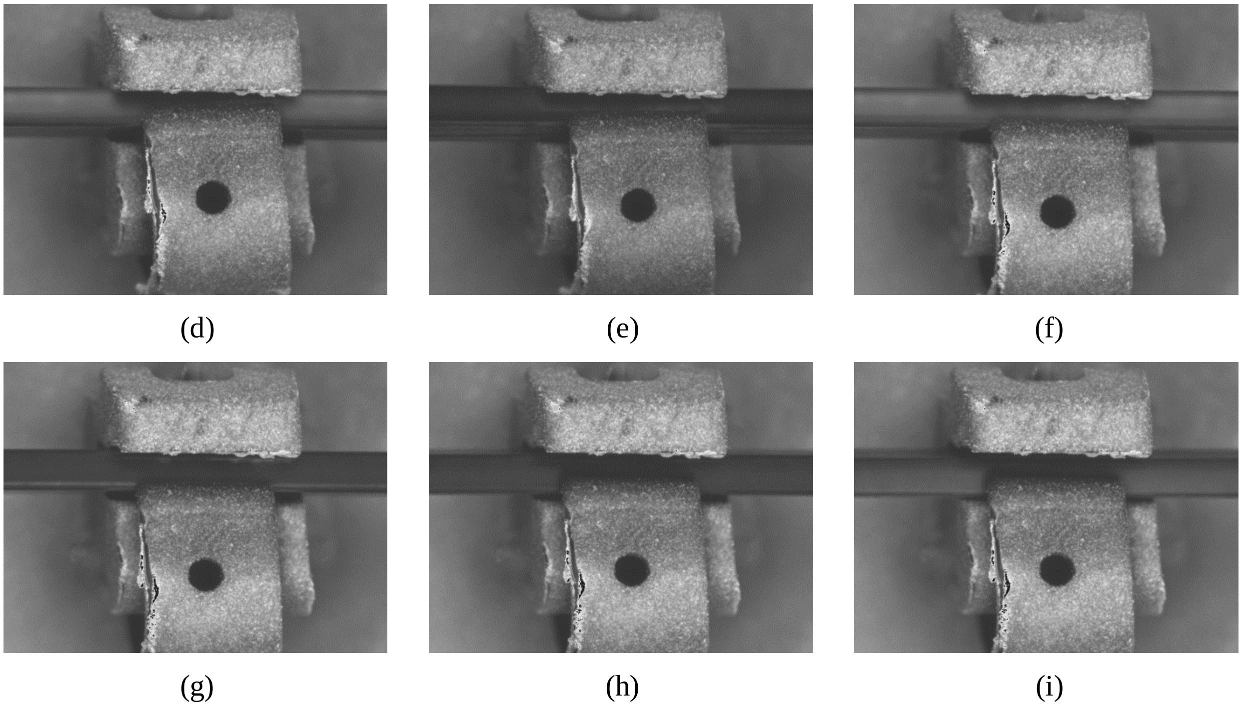

Figure 17: Speed image sequence (a) 0 degree (b) 9 degree (c) 21 degree (d) 33 degree (e) 45 degree (f) -33 degree (g) -21 degree (h) -9 degree (j) -0 degree

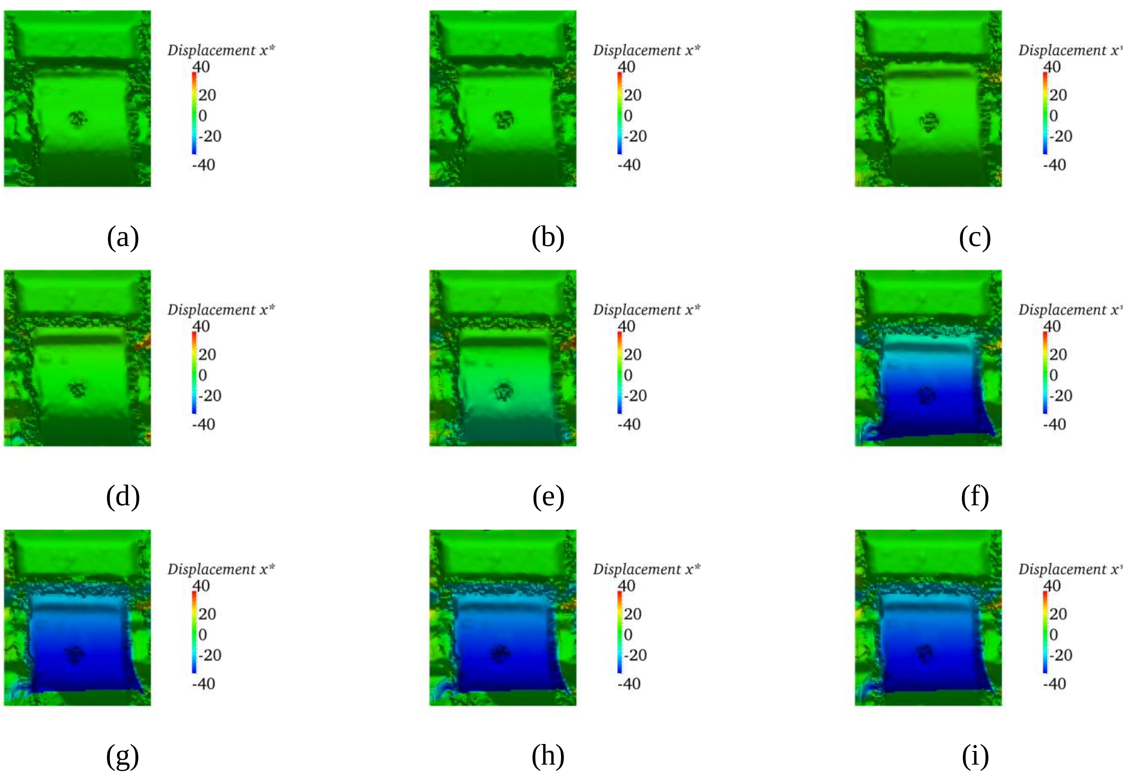

Figure 18: Speed ParaView image sequence *x displacement (a) 0 degree (b) 9 degree (c) 21 degree (d) 33 degree (e) 45 degree (f) -33 degree (g) -21 degree (h) -9 degree (j) -0 degree. Displacement measured in micrometers (µm)**

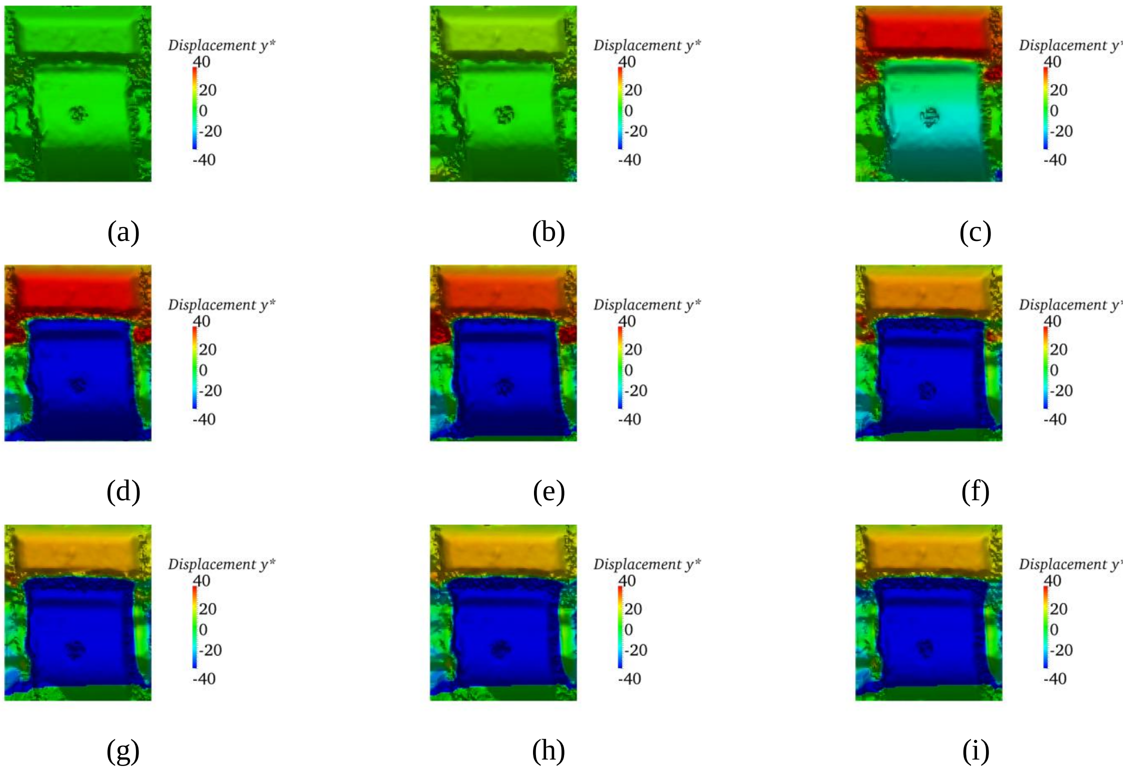

Figure 19: Speed ParaView image sequence *y displacement (a) 0 degree (b) 9 degree (c) 21 degree (d) 33 degree (e) 45 degree (f) -33 degree (g) -21 degree (h) -9 degree (j) -0 degree. Displacement measured in micrometers (µm)**

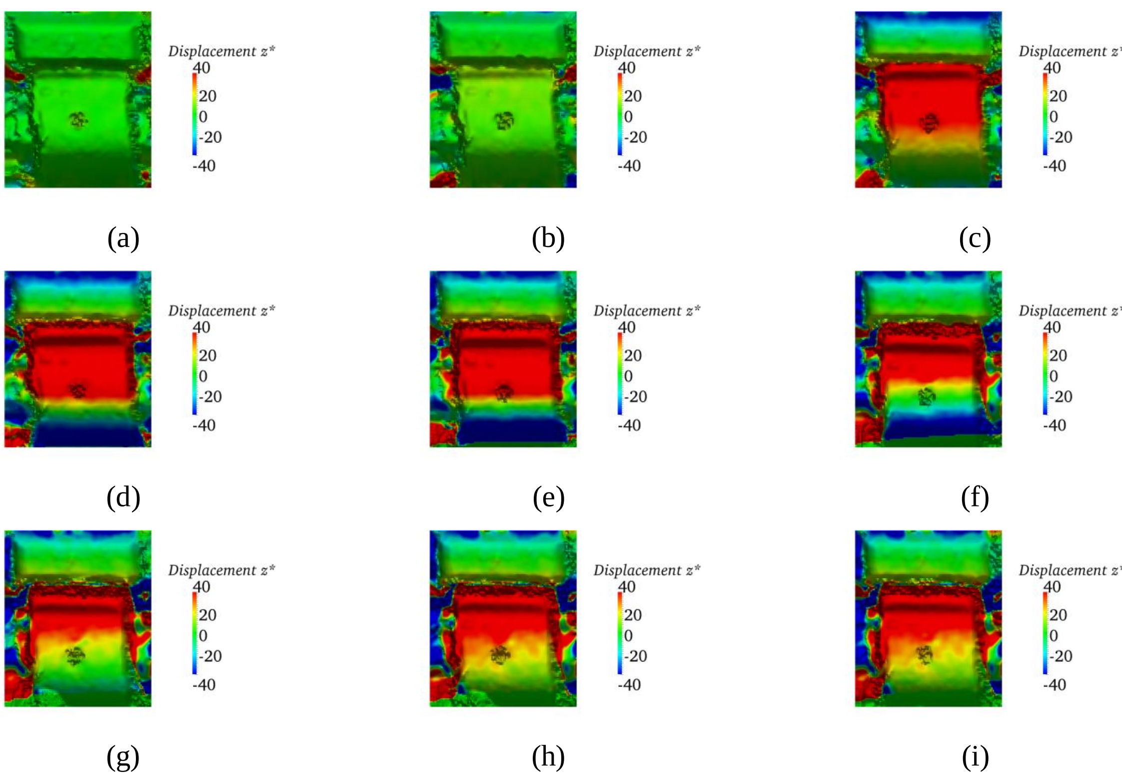

Figure 20: Speed ParaView image sequence *z displacement (a) 0 degree (b) 9 degree (c) 21 degree (d) 33 degree (e) 45 degree (f) -33 degree (g) -21 degree (h) -9 degree (j) -0 degree. Displacement measured in micrometers (µm)**

The images and contour plots of the three brackets shown in Figure 11 to Figure 20 demonstrate the 3D motion of the three brackets due to archwire rotation. The motion of the bracket tie-wings quantified using Equations (1). Comparison of the average motion of the Damon Q and In-Ovation R bracket tie-wings in the x^*,y^*,z^* directions are shown in Figure 21. Range bars in Figure 21 indicate the variation for the 8 Damon Q and 10 In-Ovation R brackets.

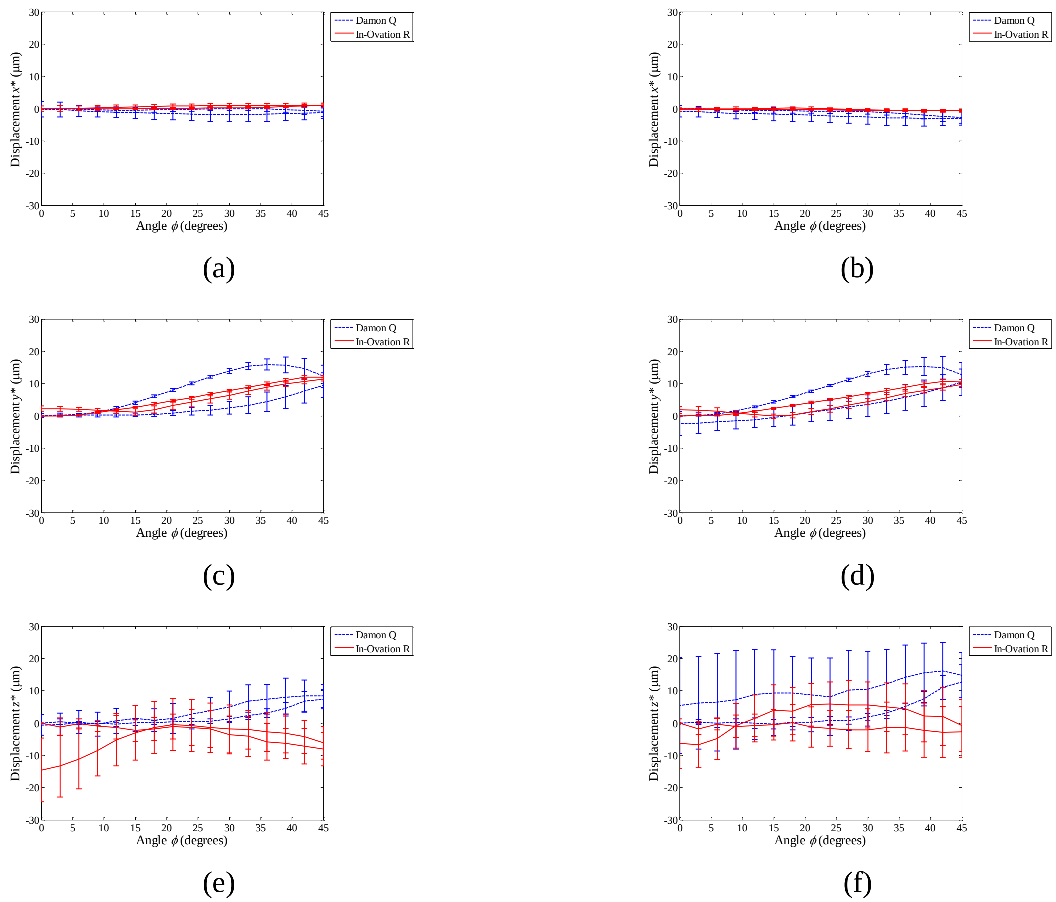

Figure 21: Comparison on Damon Q and In-Ovation R bracket tie-wing motion. Average and standard deviation displacements for (a) Tie-wing#1-3 x^* (b) Tie-wing#2-4 x^* (c) Tie-wing#1-3 y^*(d) Tie-wing#2-4 y^* (e) Tie-wing#1-3 z^* (f) Tie-wing#2-4 z^*

The average motion of the ARC of the Damon Q and In-Ovation R brackets are compared in Figure 22. The ARC motion was quantified using Equation (2). Range bars indicate the variation between each bracket tests. Figure 22 shows that the major motion for the two brackets occurs in the z^* direction.

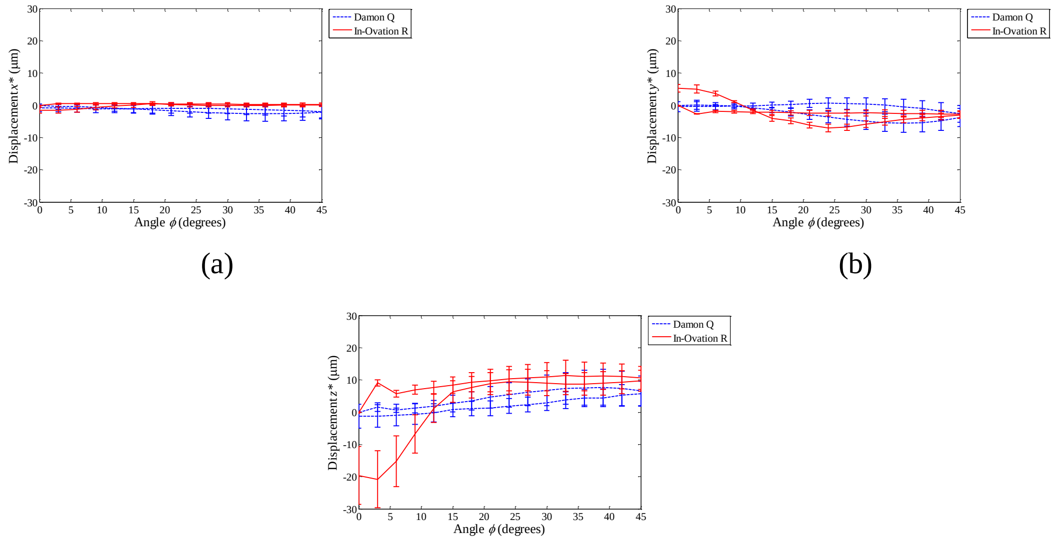

(a) (b) (c)

Figure 22: Damon Q and In-Ovation R ARC motion. Average and standard deviation of archwire retentive displacements (a) component x^* (b) ARC y^* (c) ARC z^*

4. Discussion

A total of 30 brackets were selected for the testing with the 3D OTS. For the ten (10) Damon Q brackets tested two (2) of the bracket debonded from the metal cylinder, therefore the Damon Q brackets were tested eight (8) times successfully. For the In-Ovation R brackets ten (10) tests were completed successfully. The Speed brackets were problematic. Of the ten (10) Speed bracket five (5) could not be used as the epoxy used to secure the bracket to the metal dowel adhered to the ARC as a result only five (5) brackets were available for testing. Results from the Speed brackets were not used to compare self-ligating brackets. The same gluing method was used for the Damon Q and In-Ovation R brackets as the Speed brackets and the epoxy was not found to interfere with the ARC. Figure 2 (b) and (c) shows the ARC for a Speed and In-Ovation R brackets. In this figure it can be seen that there is less clearance between the base of the bracket and the ARC for the Speed bracket than the In-Ovation R brackets. The clearance between the ARC and bracket base allows for sufficient epoxy to be applied to the bracket to ensure that the bracket does not debond during testing. In addition, the ARC of the Speed brackets opened for 4 of the tests. Therefore only one successful test was completed for the Speed brackets. A similar problem was noted by Major et al [16] for Speed brackets where the ARC opened for 16 of 30 brackets. As a result the Damon Q and In-Ovation R brackets were compared to demonstrate the difference in of passive and active ligation brackets.

The images and contour plots of the three brackets shown in Figure 11-Figure 20 demonstrate the 3D motion of the three brackets due to archwire rotation. The original bracket image sequences were processed using the 3D DIC method and then visualized using ParaView to display the deformation that occurs to the bracket due to archwire rotation. The three sets of contour plots show the different behavior of the three self-ligating brackets for the same amount of archwire rotation and highlight regions where bracket deformation occurs for the x^*,y^* and z^* directions. Also shown is the difference in magnitude of deformation across the three self-ligating brackets.

The image sequence for the Speed bracket shown in Figure 18 shows that motion of the ARC occurred in the x^* direction since the ARC opened during testing. This can be seen by comparing Figure 18 with the original image sequence in Figure 17. By contrast Figure 10 and Figure 14 show that little motion occurred in the x^* direction for the Damon Q and In-Ovation R brackets. The x^* motion for the bracket tie-wings and ARC was determined using Equation (1) and (2). The x^* tie-wing motion is shown in Figure 21 (a) and (b) and the motion in the x^* motion for the Damon and In-Ovation R brackets is less than 5μm. Similarly, the x^* ARC motion is shown in Figure 22 (a) and the measured ARC motion was found to be less than 5μm.

Significant motion can be seen for tie-wings #1 and #2 in Figure 19 for the Speed bracket and also shows that since the bracket ARC opened during testing the tie-wings did not return to the original position. The predominant motion for the bracket tie-wings is in the y^* direction for the Damon Q and In-Ovation R self-ligating brackets in Figure 21. By comparing the image sequences in Figure 11 and Figure 15 it can be seen that less deformation occurred to the In-Ovation R bracket in the y^* direction as indicated by the color gradient than the Damon Q bracket.

The z^* displacement for the Speed bracket is displayed in Figure 20 showing that the ARC displaced in the z^* direction and did not return to the original position as the archwire was returned to the starting position. The image sequence also shows that the predominant motion in the z^* direction is the ARC rather than the bracket tie-wings. The z^* motion of the Damon Q bracket was also visualized using ParaView and the resulting image sequence is shown in Figure 12. This figure shows that the greatest z^* motion occurs for the ARC of the Damon Q bracket at 45° archwire rotation. The images in Figure 12 also show that there is minimal motion in the z^* direction for the four tie-wings of the Damon Q bracket. The z^* displacement of the In-Ovation R brackets is also shown in Figure 16 where the greatest motion in the z^* direction occurs for the ARC. This contour image sequence for the In-Ovation R bracket also shows that the ARC is lower for the final bracket image compared to the initial image. The In-Ovation R brackets exhibited large variation in the z^* direction as shown in Figure 21 (e) and (f). The large z^* tie-wing variation for the In-Ovation R brackets is due to the bracket geometry. With the current stereo microscope setup the four tie-wings of the In-Ovation R brackets are difficult to keep in focus due to the shallow depth-of-focus of the stereo microscope. Major et al. [16] also described the difficulty in maintaining focus on all of the In-Ovation R bracket features. Figure 2 (c) shows the difference in height between tie-wings 1-2 and 3-4 for the In-Ovation R bracket. The variation in height between tie-wings 1-2 and 3-4 is less for the Damon Q and Speed brackets than the In-Ovation R bracket seen in Figure 2 (a) and (b). The height of the tie-wings affects the ability to focus on all four tie-wings with the stereo-microscope. Figure 21 also shows that the variation between bracket tests is much less in the x^* and y^* directions than in the z^* direction.

The calculated *P*-Values using the Mann-Whitney U nonparametric test for comparing the tie-wing motion of the two brackets are summarized in Table 1. This table compares the brackets for 45° archwire rotation and for the final deformation after the archwire has returned to the origin. From Table 1 it can be seen that a statistically signification difference exists between the two brackets in the x^* and z^* directions for 45° of wire rotation. A statistically significant difference was also detected for the final displacement in the y^* motion for both the left and right tie-wings. The average plastic deformation in the y^* direction was found to be greater for the In-Ovation R than the Damon Q bracket.

Table 1 also shows that the predominant motion for the bracket tie-wings occurs in the y^* direction. For the Damon Q bracket the magnitude of y^* motion was 13.7 and 4.8 times greater than the x^* motion for tie-wings#1-3 and #2-4. As well the magnitude of y^* motion was 1.67 and 0.96 times greater than the z^* motion for tie-wings#1-3 and #2-4. Similarly, the In-Ovation y^* motion was 13.2 and 14.4 times greater than the x^* motion for tie-wings#1-3 and #2-4. Also, the y* motion was 1.5 and 3.8 times greater than the z* motion for the In-Ovation R bracket. Table 1 and Figure 21 show that the most displacement occurs in the y^* direction for the bracket tie-wings due to archwire rotation. Therefore, the y^* motion should be used to assess variations between bracket tie-wing designs.

Table 1: Maximum and plastic deformation due to archwire rotation for Damon Q and In-Ovation R brackets. Bolded values show significant differences.

Bracket Tie-wing	Maximum Average Displacement (μm)			Plastic Deformation (μm)		
	Damon Q	In-Ovation R	*P*-Value	Damon Q	In-Ovation R	*P*-Value
Tie-wing#1-3 x^* (stdev)	-0.89(1.55)	0.91(0.52)	**0.014**	-0.20(2.37)	-0.05(0.82)	0.3822
Tie-wing#2-4 x^* (stdev)	-2.71(1.83)	-0.73(0.38)	**0.010**	-0.81(1.81)	-0.36(0.54)	0.6453
Tie-wing#1-3 y^* (stdev)	12.21(3.50)	12.00(0.57)	0.959	0.09(0.63)	2.20(0.82)	**0.0001**
Tie-wing#2-4 y^* (stdev)	12.67(3.86)	10.48(0.71)	0.050	-2.46(3.74)	1.82(1.14)	**0.0206**
Tie-wing#1-3 z^* (stdev)	7.31(2.98)	-8.08(5.26)	**0.0001**	-0.61(3.21)	-14.60(9.88)	**0.0018**
Tie-wing#2-4 z^* (stdev)	12.71(5.46)	-2.70(7.85)	**0.0003**	5.37(14.86)	-6.32(7.65)	0.1303

The z^* motion of the ARC for the In-Ovation R bracket, shown in Figure 22 (c), shows a sharp increase at 3° archwire rotation. This increase is due to the initial contact of the archwire with the ARC. The ARC z^* displacement continues to increase after 3° of archwire rotation. As the archwire reached 20-25° wire rotation the z^* motion of the ARC began to plateau. The plateau seen for the In-Ovation R z^* motion is most likely due to the ARC contacting the "slot blocker" or small slots where the ARC is retained by the tie-wings shown in Figure 2 (c) and Figure 3 (b) which prevents the ARC from becoming separated from the bracket tie-wings. By contrast a sharp increase is not seen in the ARC of the Damon Q brackets.

The calculated P-Values for comparing the ARC motion of the two brackets are summarized in Table 2. This table compares the brackets for 45° archwire rotation and for the final deformation after the archwire has returned to the original position. From Table 2 it can be seen that a statistically signification difference exists between the two brackets in the x^* and z^* directions for 45° of wire rotation. A statistically significant difference was also detected for the final displacement in the y^* and z^* ARC motion. The magnitude of motion in the z^* direction is 2.2 and 2.9 times greater than the x^* and y^* direction for the Damon Q ARC. As well, motion in the z* direction for the In-Ovation R bracket is 81.4 and 3.18 times greater than the x^* and y^* directions. Therefore, the z^* motion should be used to assess variations between bracket ARC designs. The final position of the ARC for the In-Ovation R bracket is much less than the Damon Q bracket. This is indicated by the significant difference in final z^* position in Table 2. Comparison of the final position of the ARC of the Damon Q and In-Ovation R is also shown in Figure 22. The final position of the ARC of the In-Ovation R bracket is due to the compliance of the ARC which causes the ARC to encroach the bracket slot [25]. The large final displacement of the ARC is also shown in the contour plot of the In-Ovation R bracket in Figure 16.

Table 2: Maximum ARC motion.

ARC Displacement	Maximum Average Displacement (μm)			Final Deformation (μm)		
	Damon Q	In-Ovation R	P-Value	Damon Q	In-Ovation R	P-Value
x^* (stdev) [μm]	-1.95(1.93)	0.12(0.55)	**0.0046**	-0.77(1.18)	-1.56(0.91)	0.3822
y^* (stdev) [μm]	-2.63(2.63)	-3.07(1.05)	0.8784	-0.39(1.55)	5.29(1.15)	**0.0002**
z^* (stdev) [μm]	5.70(3.91)	9.77(3.28)	**0.0379**	-1.23(3.75)	-19.62(8.99)	**0.0002**

There has been limited investigation into the behavior of the ARC [26]. Pandis et al. [27] examined the deformation and change in stiffness of the ARC of two active ligation brackets by measuring the force applied by the ARC. An archwire was displaced labially in the bracket slot in 0.02mm (20μm) increments to a maximum displacement of 1.5mm and the force applied by the ARC was measured at each increment. This motion is well beyond the displacement that was seen for a typical bracket due to archwire rotation using the OTS. Figure 22 shows that for a maximum archwire rotation of 45° the ARC displaced 9.77μm for the In-Ovation R bracket and 5.70μm for the Damon Q bracket. The displacement of the ARC measured using the 3D OTS was found to be 2.0 and 3.5 times less for the In-Ovation and Damon Q brackets than the initial displacement used by Pandis et al. [27]. Using the 3D OTS it will be possible to evaluate effects such as cyclic loading on the ARC to determine if loading over time affects the mechanical properties of the ARC.

5. **Conclusion**

A non-contact measurement method has been developed to evaluate the 3D motion of orthodontic brackets. This method has been used to measure the displacement of two self-ligating brackets to measure tie-wing and ARC motion. The motion of the ARC has not been extensively evaluated for self-ligating brackets nor has the 3D motion of bracket tie-wings. The 3D OTS allows for the 3D motion of the ARC to be measure in response to archwire rotation and can be used to determine the compliance of the ARC. Contour plots of three self-ligating brackets have been created using data acquired using a 3D DIC method. The contour plots visualize the displacement that occurs to the orthodontic brackets due to progressive archwire rotation and can be used to demonstrate regions where large deformation occurs. The displacement of the ARC measured using the 3D OTS was found to be 2.0 and 3.5 times less for the In-Ovation and Damon Q brackets than previous studies used to examine the compliance of the ARC.
Investigation the motion of the bracket tie-wings for the Damon Q and In-Ovation R bracket has shown the magnitude of y^* motion was greater than the x^* and z^* tie-wing motion due to archwire rotation. Therefore, the y^* motion should be used for comparison of bracket designs and there 3D DIC measurement method is not necessary to compare bracket tie-wing motion since the single camera 2D DIC method is capable of measuring the y^* tie-wing motion. Conversely, the z^* motion of the ARC was found to be greater than the x^* and y^* motion for both the Damon Q and In-Ovation R brackets. As a result there stereo microscope version of the OTS should be used to compare the compliance of the ARC of self-ligating brackets.

6. **References**

References

[1] W. R. Proffit, H. W. Fields and D. M. Sarver, *Contemporary Orthodontics.* St. Louis, Mo.: Mosby Elsevier, 2007.

[2] R. Nanda and A. Kuhlberg, "Principles of biomechanics," in *Biomechanics in Clinical Orthodontics*, R. Nanda, Ed. Philadelphia, PA: Saunders, 1997, pp. 1-20.

[3] D. A. Flores, L. K. Choi, J. M. Caruso, J. L. Tomlinson, G. E. Scott and M. T. Jeiroudi, "Deformation of metal brackets: a comparative study." *Angle Orthod.*, vol. 64, pp. 283-290, 1994.

[4] J. Odegaard, T. Meling and E. Meling, "An evaluation of the torsional moments developed in orthodontic applications. An in vitro study." *Am. J. Orthod. Dentofacial Orthop.*, vol. 105, pp. 392-400, 1994.

[5] H. Gmyrek, C. Bourauel, G. Richter and W. Harzer, "Torque capacity of metal and plastic brackets with reference to materials, application, technology and biomechanics," *Journal of Orofacial Orthopedics,* vol. 63, pp. 113-128, 2002.

[6] R. Lacoursiere, D. Nobes, D. Homeniuk, J. P. Carey, H. Badawi and P. W. Major. Measurement of orthodontic bracket tie wing elastic and plastic deformation by arch wire torque expression utilizing an optical image correlation technique. *Journal of Dental Biomechanics vol. 2010(Article ID 397037),* 2010.

[7] H. M. Badawi, R. W. Toogood, J. P. R. Carey, G. Heo and P. W. Major, "Torque expression of self-ligating brackets," *American Journal of Orthodontics and Dentofacial Orthopedics,* vol. 133, pp. 721-728, 2008.

[8] W. H. Peters and W. F. Ranson, "Digital Imaging Techniques in Experimental Stress Analysis," *Optical Engineering,* vol. 21, pp. 427-431, 1982.

[9] T. C. Chu, W. F. Ranson and M. A. Sutton, "Applications of digital-image-correlation techniques to experimental mechanics," *Exp. Mech.*, vol. 25, pp. 232-244, 1985.

[10] H. A. Bruck, S. R. McNeill, M. A. Sutton and W. H. Peters III, "Digital image correlation using Newton-Raphson method of partial differential correction," *Exp. Mech.*, vol. 29, pp. 261-267, 1989.

[11] M. A. Sutton, J. L. Turner, H. A. Bruck and T. A. Chae, "Full-field representation of discretely sampled surface deformation for displacement and strain analysis," *Exp. Mech.*, vol. 31, pp. 168-177, 1991.

[12] F. Hild and S. Roux, "Digital image correlation: From displacement measurement to identification of elastic properties - A review," *Strain,* vol. 42, pp. 69-80, 2006.

[13] B. Pan, K. Qian, H. Xie and A. Asundi, "Two-dimensional digital image correlation for in-plane displacement and strain measurement: A review," *Measurement Science and Technology,* vol. 20, 2009.

[14] M. A. Sutton, J. J. Orteu and H. W. Schreier, *Image Correlation for Shape, Motion and Deformation Measurements : Basic Concepts, Theory and Applications*. New York, N.Y: Springer, 2009.

[15] J. Li, A. S. L. Fok, J. Satterthwaite and D. C. Watts, "Measurement of the full-field polymerization shrinkage and depth of cure of dental composites using digital image correlation," *Dental Materials,* vol. 25, pp. 582-588, 2009.

[16] T. W. Major, J. P. Carey, D. S. Nobes, G. Heo and P. W. Major, "Measurement of plastic and elastic deformation due to third-order torque in self-ligated orthodontic brackets," *Am. J. Orthod. Dentofacial Orthop.*, vol. 140, pp. 326-339, Sep, 2011.

[17] T. W. Major, J. P. Carey, D. S. Nobes, G. Heo, G. W. Melenka and P. W. Major, "An investigation into the mechanical characteristics of select self-ligated brackets at a series of clinically relevant

maximum torquing angles: loading and unloading curves and bracket deformation," *Eur. J. Orthod.*, Jul 12, 2011.

[18] G. W. Melenka, R. A. Lacoursiere, J. P. Carey, D. S. Nobes, G. Heo and P. W. Major, "Comparison of deformation and torque expression of the orthos and orthos Ti bracket systems," *Eur. J. Orthod.*, Oct 19, 2011.

[19] P. F. Luo, Y. J. Chao, M. A. Sutton and W. H. Peters III, "Accurate measurement of three-dimensional deformations in deformable and rigid bodies using computer vision," *Exp. Mech.*, vol. 33, pp. 123-132, 1993.

[20] D. Garcia, J. J. Orteu and L. Penazzi, "A combined temporal tracking and stereo-correlation technique for accurate measurement of 3D displacements: Application to sheet metal forming," *J. Mater. Process. Technol.*, vol. 125-126, pp. 736-742, 2002.

[21] J. -. Orteu, "3-D computer vision in experimental mechanics," *Opt Lasers Eng*, vol. 47, pp. 282-291, 2009.

[22] W. A. Brantley and T. Eliades, "Orthodontic brackets," in *Orthodontic Materials: Scientific and Clinical Aspects*, W. A. Brantley and T. Eliades, Eds. New York: Thieme, 2001, pp. 144-147,165.

[23] N. Harradine, "Self-ligating brackets: Theory, practice, and evidence," in *Orthodontics : Current Principles and Techniques*, 5th ed., L. W. Graber, Ed. Philadelphia, PA: Elsevier/Mosby, 2012, pp. 581.

[24] G. A. Thorstenson and R. P. Kusy, "Effect of archwire size and material on the resistance to sliding of self-ligating brackets with second-order angulation in the dry state," *American Journal of Orthodontics and Dentofacial Orthopedics*, vol. 122, pp. 295-305, 2002.

[25] N. W. Harradine, "Self-ligating brackets: where are we now?" *J. Orthod.*, vol. 30, pp. 262-273, 2003.

[26] N. W. Harradine, "Historical aspects and evolution of ligation and appliances," in *Self-Ligation in Orthodontics: An Evidence-Based Approach to Biomechanics and Treatment*, T. Eliades and N. Pandis, Eds. Chichester, U.K. ; Ames, Iowa: Wiley-Blackwell, 2009, pp. 1.

[27] N. Pandis, C. Bourauel and T. Eliades, "Changes in the stiffness of the ligating mechanism in retrieved active self-ligating brackets," *American Journal of Orthodontics and Dentofacial Orthopedics*, vol. 132, pp. 834-837, 2007.

[28] N. Pandis, T. Eliades and C. Bourauel, "Biomechanics of self-ligation: Analysis of forces and moments exerted by self-ligating brackets," in *Self-Ligation in Orthodontics: An Evidence-Based Approach to Biomechanics and Treatment*, T. Eliades and N. Pandis, Eds. Chichester, U.K. ; Ames, Iowa: Wiley-Blackwell, 2009, pp. 33-44.

[29] LaVision GmbH, "Product-Manual for DaVis 7.2 StrainMaster Software Item-Number(s): 1105022," 2006.

[30] B. Pan, K. Qian, H. Xie and A. Asundi, "Two-dimensional digital image correlation for in-plane displacement and strain measurement: A review," *Meas Sci Technol*, vol. 20, 2009.

[31] T. A. Berfield, J. K. Patel, R. G. Shimmin, P. V. Braun, J. Lambros and N. R. Sottos, "Micro-and nanoscale deformation measurement of surface and internal planes via digital image correlation," *Exp. Mech.*, vol. 47, pp. 51-62, 2007.